

# Observations of V838 Mon in the CO rotational transitions

T. Kamiński<sup>1</sup>, M. Miller<sup>2</sup>, R. Tylenda<sup>1</sup>

<sup>1</sup> Department for Astrophysics, N. Copernicus Astronomical Centre, Radańska 8, 87-100 Toruń, Poland  
e-mail: tomkam@ncac.torun.pl

<sup>2</sup> I. Physikalisches Institut, Universität zu Köln, Zùlpicher Strasse 77, 50937 Köln, Germany

Received; accepted

## ABSTRACT

**Aims.** We investigate the structure of a field around the position of V838 Mon as seen in the lowest CO rotational transitions. We also measure and analyse emission in the same lines at the position of V838 Mon.

**Methods.** Observations have primarily been done in the  $^{12}\text{CO } J = 2 \rightarrow 1$  and  $J = 3 \rightarrow 2$  lines using the KOSMA telescope. A field of 3.4 squared degrees has been mapped in the on-the-fly mode in these transitions. Longer integration spectra in the on-off mode have been obtained to study the emission at the position of V838 Mon. Selected positions in the field have also been observed in the  $^{12}\text{CO } J = 1 \rightarrow 0$  transition using the Delingha telescope.

**Results.** In the observed field we have identified many molecular clouds. They can be divided into two groups from the point of view of their observed radial velocities. One, having  $V_{\text{LSR}}$  in the range 18 – 32 km s<sup>-1</sup>, can be identified with the Perseus Galactic arm. The other one, having  $V_{\text{LSR}}$  between 44 – 57 km s<sup>-1</sup>, probably belongs to the Norma-Cygnus arm. The radial velocity of V838 Mon is within the second range but the object does not seem to be related to any of the observed clouds. We did not find any molecular bubble of a 1° dimension around the position of V838 Mon claimed in van Loon et al. An emission has been detected at the position of the object in the  $^{12}\text{CO } J = 2 \rightarrow 1$  and  $J = 3 \rightarrow 2$  transitions. The emission is very narrow (FWHM  $\approx 1.2$  km s<sup>-1</sup>) and at  $V_{\text{LSR}} = 53.3$  km s<sup>-1</sup>. Our analysis of the data suggests that the emission is probably extended.

**Key words.** stars: individual: V838 Mon – stars: peculiar – radio lines: stars – radio lines: ISM – ISM: clouds – ISM: molecules

## 1. Introduction

The outburst of V838 Mon was discovered in the beginning of January 2002. Initially thought to be a nova, the object appeared unusual and enigmatic in its nature. The eruption, as observed in the optical, lasted about three months (Munari et al. 2002, Kimeswenger et al. 2002, Crause et al. 2003). After developing an A–F supergiant spectrum at the maximum at the beginning of February 2002, the object evolved to lower effective temperatures and in April 2002 it practically disappeared from the optical, remaining very bright in the infrared. A detailed analysis of the evolution of the object in the outburst and decline can be found in Tylenda (2005).

Different outburst mechanisms have been proposed to explain the eruption of V838 Mon. They include an unusual nova (Iben & Tutukov 1992), a late He-shell flash (Lawlor 2005) and a stellar merger (Soker & Tylenda 2003). These models have critically been discussed in Tylenda & Soker (2006) and the authors conclude that the only mechanism that can satisfactorily account for the observational data is a collision and merger of a low-mass pre-main-sequence star with an  $\sim 8 M_{\odot}$  main-sequence star.

V838 Mon is surrounded by diffuse matter which gave rise to a spectacular light-echo phenomenon (e.g. Bond et al. 2003). Bond et al. claim that the matter comes from previous eruptions of the object. However Tylenda (2004), Crause et al. (2005), as well as Tylenda, Soker & Szczerba (2005) argue that the echoing matter is of interstellar origin. The latter is consistent with recent findings, namely that V838 Mon is a member of a young open cluster (Afsar & Bond 2007) and that the total mass of the

echoing matter is probably of the order of 100  $M_{\odot}$  (Banerjee et al. 2006).

van Loon et al. (2004) have analyzed archive infrared and radio data on the sky around V838 Mon and claimed discovery of multiple shells ejected by the object in the past. In particular, from a compilation of CO galactic surveys done in Dame et al. (2001) van Loon et al. have suggested that V838 Mon is situated within a bubble of CO emission with a diameter of  $\sim 1^{\circ}$ . These results have been critically discussed in Tylenda et al. (2005), who have concluded that the shells of van Loon et al. are not realistic.

Deguchi et al. (2005) have discovered an SiO maser emission from V838 Mon. The main component is narrow and centered at  $V_{\text{LSR}} \approx 54$  km s<sup>-1</sup>, which is thought to be a radial velocity of the object itself. Further observations of Claussen et al. (2007) have shown that the SiO maser is variable and that most of the emission comes from a region smaller than a milliarcsecond.

In the present paper we report on results of our observations of V838 Mon and its nearby vicinity in the  $^{12}\text{CO } J = 1 \rightarrow 0$ ,  $2 \rightarrow 1$  and  $3 \rightarrow 2$  transitions. We describe the observational material and discuss results on the CO emission from a field of 3.4 squared degrees around the position of V838 Mon. One of the goal of this survey is to verify the existence of the CO bubble around V838 Mon claimed in van Loon et al. (2004). Measurements of the CO emission obtained at the position of V838 Mon are also presented, analysed and discussed. A preliminary analysis of the data has been done in Kamiński et al. (2007).

**Table 1.** Technical characteristics of the observations in the rotational transitions of CO.

CO line telescope	$J = 1 \rightarrow 0$ Delingha	$J = 2 \rightarrow 1$ KOSMA	$J = 3 \rightarrow 2$ KOSMA
HPBW <sup>a</sup>	55''	130''	82''
$T_{\text{sys}}$ DSB <sup>b</sup> [K]	230 $\div$ 290	150 $\div$ 230	230 $\div$ 380
vel. range [km s <sup>-1</sup> ]	-139 $\div$ 239	-106 $\div$ 216	-121 $\div$ 231
$\Delta V_{\text{ch}}$ [km s <sup>-1</sup> ]	0.37	0.22	0.29
$\eta_{\text{mb}}$	0.63	0.68	0.79
$\langle \sigma_{\text{rms}} \rangle^c$ [K]	0.14	0.42	0.93

<sup>a</sup> half power beam width of the main beam

<sup>b</sup> double-side band system temperature including the atmospheric contribution

<sup>c</sup> average sensitivity given in the main beam scale

## 2. Observations

Most of the data analysed in the present study were obtained with the 3 m Kölner Observatorium für Sub-Millimeter Astronomie (KOSMA) telescope in the  $^{12}\text{CO}$   $J = 2 \rightarrow 1$  (230.54 GHz) and  $J = 3 \rightarrow 2$  (345.80 GHz) transitions. They include maps covering an area around the position of V838 Mon as well as several long integration measurements at the position of the object. Complementary observations in the  $^{12}\text{CO}$   $J = 1 \rightarrow 0$  (115.27 GHz) transition have been obtained using the 13.7 m Delingha telescope at the Purple Mountain Observatory (China). Basic technical details of the measurements are summarised in Table 1.

### 2.1. Observations with the KOSMA telescope

The main observations mapping an area of 3.4 squared degrees around the position of V838 Mon were acquired on 1-5 April 2005. The maps were obtained in the on-the-fly observing mode (Kramer et al. 1999, Beuther et al. 2000) with a sampling of 1' and with an emission-free reference position at  $\alpha_{2000} = 07^{\text{h}} 07^{\text{m}} 00^{\text{s}}$ ,  $\delta_{2000} = -03^{\circ} 15' 00''$ . Observations resulted in a set of 12 400 spectra in each of the two transitions ( $2 \rightarrow 1$  and  $3 \rightarrow 2$ ). Typical integration time was of 4 s.

Figure 1 shows a  $3^{\circ}5' \times 3^{\circ}5'$  map centered at the V838 Mon position taken from the Dame et al. (2001) compilation of CO ( $1 \rightarrow 0$ ) surveys. The region mapped in our observations is shown with a solid line.

A number of long integration spectra in both transitions at the position of V838 Mon were obtained on 4 April 2005 and 26 December 2005. On 16-19 April 2006 observations were done only in the ( $2 \rightarrow 1$ ) line, but apart from the object position, 6 nearby positions with offsets (0, 1), (0, 2), (0, -1), (0, -2), (-2, 0), and (2, 0) ( $\Delta\alpha$ ,  $\Delta\delta$  – in arcmin, relative to the V838 Mon position) were also observed.

During the observations the KOSMA telescope (Kramer et al. 1998) was equipped with a dual-channel SIS receiver (Graf et al. 1998) with a bandwidth of 1 GHz. The receiver was connected to acousto-optical spectrometers of medium and variable resolution (Schieder et al. 1989) with a channel spacing (bandwidth) of 165.4 kHz (248 MHz) and 339 kHz (407 MHz) for the CO ( $2 \rightarrow 1$ ) and ( $3 \rightarrow 2$ ) data sets, respectively. The system temperature was changing significantly during the observations mainly due to variable atmospheric conditions. It was in a range of 150–230 K at 230 GHz and 230–380 K at 345 GHz. Pointing scans on planets were carried out every 2–3 hours and the

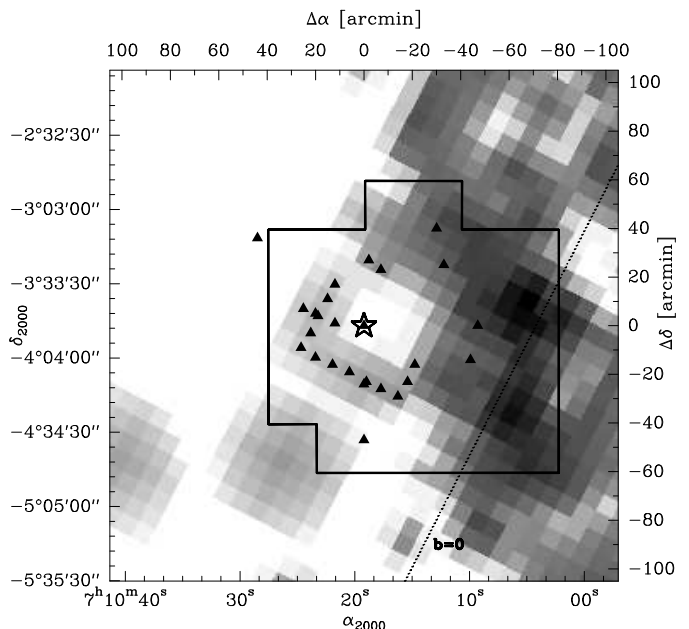


**Fig. 1.** A  $3^{\circ}5' \times 3^{\circ}5'$  map centered at the V838 Mon position from the Dame et al. (2001) compilation of CO ( $1 \rightarrow 0$ ) surveys (the data taken from SkyView – <http://skyview.gsfc.nasa.gov/>). The star symbol marks the position of V838 Mon. The polygon drawn with a solid line shows the region mapped in our KOSMA on-the-fly observations in the CO ( $2 \rightarrow 1$ ) and ( $3 \rightarrow 2$ ) transitions. Filled triangles mark the positions observed with the Delingha telescope in the CO ( $1 \rightarrow 0$ ) transition. Dashed line indicates the Galactic equator. The upper and right axes show the offsets in arcminutes from the position of V838 Mon.

pointing accuracy was better than about 10''. The data were calibrated using the standard chopper wheel method (Kutner & Ulich 1981) giving spectra in the antenna temperature,  $T_{\text{A}}^*$  (e.g. Rohlfs & Wilson 2004), corrected for atmospheric attenuation, ohmic losses, rearward spillover and scattering. In order to remove significant instrumental baseline effects, polynomial baselines up to fourth order were subtracted.

### 2.2. Observations with the Delingha telescope

Observations in the  $^{12}\text{CO}$   $J = 1 \rightarrow 0$  transition were conducted on 28 October – 3 November 2005. 25 points around the object were measured. All the points are shown with triangles in Fig. 1. As can be seen from Fig. 1, most of the points are located in the bubble-like structure claimed in van Loon et al. (2004). The position of V838 Mon as well as 8 nearby positions with offsets (0, 1), (-1, 1), (-1, 0), (-1, -1), (0, -1), (1, -1), (1, 0), and (1, 1) ( $\Delta\alpha$ ,  $\Delta\delta$  – in arcmin, relative to the V838 Mon position) have also been measured. The integration time was 5 minutes for the object position and 1 minute per each of the 8 offset positions.

All the Delingha observations were done in the position switching mode with a reference position at  $\alpha_{2000} = 07^{\text{h}} 07^{\text{m}} 01^{\text{s}}$ ,  $\delta_{2000} = -03^{\circ} 14' 51''$ . Each point was observed with an integration time of 4 – 8 min. A heterodyne SIS receiver and an acousto-optical spectrograph have been used as frontend and backend, respectively. A typical system temperature was of 260 K (DSB, including sky contribution). Bandwidth and channel spacing were 145.5 MHz and 142 kHz, respectively. Pointing of the antenna was regularly checked by observing

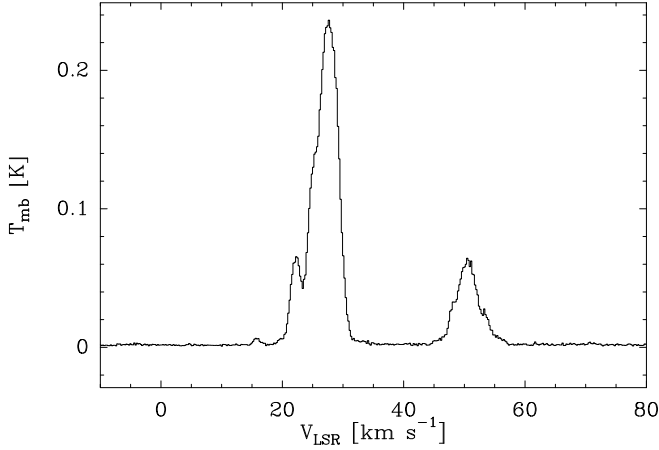


**Fig. 2.** The mean spectrum obtained from averaging over all the observed positions in the  $J = 2 \rightarrow 1$  transition.

planets and SiO masers at 86 GHz and had an accuracy of  $6''$ . The observations were calibrated and expressed in the antenna temperature scale. From the resulting spectra low order polynomial baselines were subtracted.

Most of the results presented in the next section are in the scale of the main beam temperature,  $T_{\text{mb}}$ . This is related to the antenna temperature as  $T_{\text{mb}} = T_{\text{A}}^*/\eta_{\text{mb}}$ , where  $\eta_{\text{mb}}$  is the main beam efficiency given for each transition in Table 1. Beamwidths of the antennas at the appropriate frequencies are also presented in the table. The last row in Table 1 gives the sensitivity of our observations in terms of an average baseline-noise rms of the spectra. All velocities in this paper are given with respect to the local standard of rest (LSR).

All the data reduction as well as the analysis of the results have been done using the GILDAS<sup>1</sup> software.

### 3. Maps of the field around the V838 Mon position

The observations with the KOSMA telescope provided us with a total number of 24800 spectra in the  $J = 2 \rightarrow 1$  and  $3 \rightarrow 2$  transitions. The resultant maps in both transitions are qualitatively similar. The survey in  $J = 2 \rightarrow 1$  was however more sensitive (see Table 1) and gave more details in the maps, so most of the discussion and estimates done in the present section will be based on the  $J = 2 \rightarrow 1$  survey.

Figure 2 shows a mean spectrum obtained from averaging over all the observed positions in the  $J = 2 \rightarrow 1$  transition. As can be seen, a significant signal has been detected in two well separated ranges of  $V_{\text{LSR}}$ , namely 18 – 32 and 44 – 57  $\text{km s}^{-1}$ . As discussed in Appendix A, they correspond to two populations of interstellar clouds belonging to two different spiral arms (Perseus arm and Norma-Cygnus arm, respectively) of the Galaxy. The second velocity range (44–57  $\text{km s}^{-1}$ ) is more interesting from the point of view of V838 Mon. The presumable radial velocity of the object, as inferred e.g. from the SiO maser emission, is within this range.

Figure 3 presents a map of the  $J = 2 \rightarrow 1$  emission integrated over the  $V_{\text{LSR}}$  range 18 – 32  $\text{km s}^{-1}$ . The same but for the  $V_{\text{LSR}}$  range 44 – 57  $\text{km s}^{-1}$ , is shown in Fig. 4. Channel maps derived

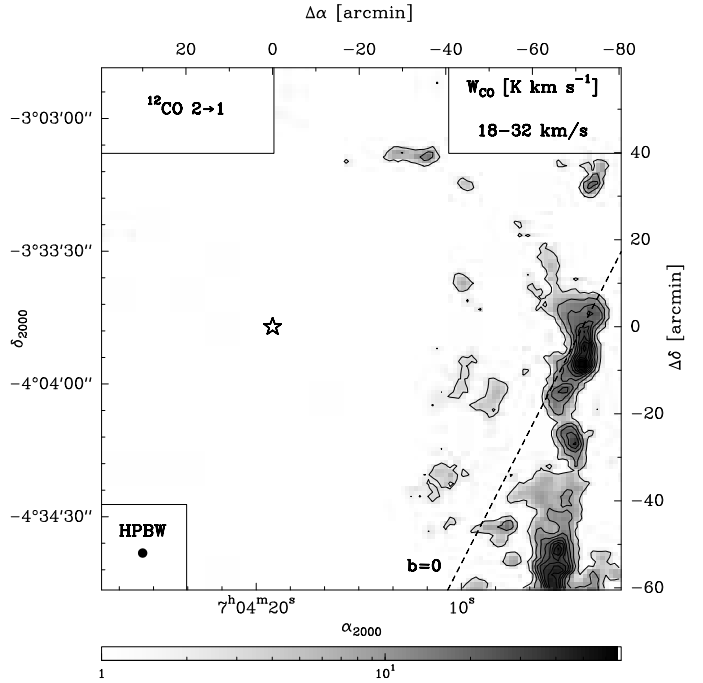


**Fig. 3.** The intensity map of CO  $J = 2 \rightarrow 1$  integrated over a the  $V_{\text{LSR}}$  range 18–32  $\text{km s}^{-1}$ . Contours are plotted from 2.7 to 63.8  $\text{K km s}^{-1}$  with a spacing of 6.8  $\text{K km s}^{-1}$  (4 to 94% spaced with 10% of the maximum). The star-like symbol indicates the V838 Mon position. The Galactic equator is shown as a dashed line.

from integrations over narrower velocity ranges, both in the  $J = 2 \rightarrow 1$  and  $3 \rightarrow 2$  transitions, as well as a detailed discussion of the molecular clouds identified from the maps, can be found in Appendix A.

#### 3.1. On the bubble-like structure of van Loon et al. (2004)

As mentioned in Sect. 1 one of our motivations to observe the surroundings of V838 Mon in the CO rotational lines was the claim of van Loon et al. (2004) that the object is situated in a bubble-like structure of  $\sim 1^\circ$  in diameter seen in the CO (1 $\rightarrow$ 0) transition. As can be easily seen from our maps in the (2 $\rightarrow$ 1) line no structure of this kind is present (see Figs. 3 and 4). In particular, if the structure were real and related to V838 Mon it should have been present in the  $V_{\text{LSR}}$  range presented in in Fig. 4, which is not the case.

Most of our observations obtained with the Delingha telescope were meant to further investigate this problem. These measurements were done in the CO (1 $\rightarrow$ 0) transition, i.e. in the same line in which the map investigated by van Loon et al. had been done, and the observed positions were chosen to probe the structure of van Loon et al. (see Fig. 1). Note also that the Delingha observations were significantly more sensitive than the KOSMA maps (see Table 1).

A significant emission at a level of 4–8  $\text{K km s}^{-1}$  was detected at 4 positions with the following  $(\alpha, \delta)$  offsets (in arcmin) relative to the V838 Mon position: (–30, 40), (–33, 25), (–44, –14), and (–47, 0) (4 rightmost triangles in Fig. 1). These detections are within the emission regions seen in our (2 $\rightarrow$ 1) maps obtained with KOSMA (Figs. 3 and 4). A less significant emission at a level of 0.6–1.5  $\text{K km s}^{-1}$  was also found at (–7, 23), (12, 1), and (6, –19). No emission at

<sup>1</sup> Grenoble Image and Line Data Analysis Software, [www.iram.fr/IRAMFR/GILDAS](http://www.iram.fr/IRAMFR/GILDAS)

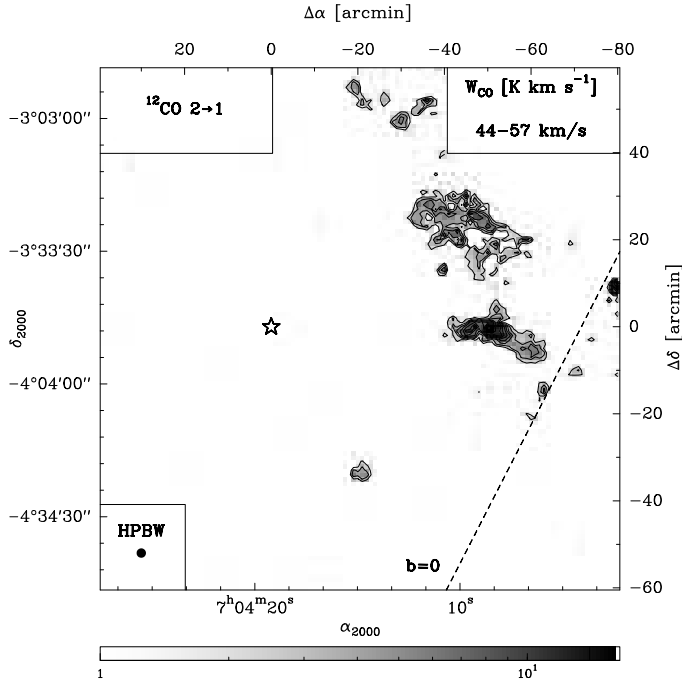


**Fig. 4.** The same as Fig. 3 but integrated over the  $V_{\text{LSR}}$  range 44–57  $\text{km s}^{-1}$ . Contours are plotted from 2.3 to 15.5  $\text{K km s}^{-1}$  with a spacing of 1.6  $\text{K km s}^{-1}$  (14 to 94% spaced with 10% of the maximum).

the latter positions was detected in the KOSMA survey, most probably due to a lower sensitivity of the latter. No emission in the (1→0) transition was detected at any other of the remaining 18 positions observed with the Delingha telescope.

We can thus conclude that our data do not confirm the existence of the CO bubble-like structure claimed in van Loon et al. (2004). Note that this structure was not seen in any other domain, in particular in the IRAS maps (e.g. Tylenda et al. 2005). As discussed in Tylenda et al. (2005), the CO bubble of van Loon et al. was likely to be an artefact of merging two surveys of different resolution and sensitivity in the compilation of Dame et al. (2001).

## 4. Observations at the position of V838 Mon

### 4.1. Results from the KOSMA telescope

The on-the-fly observations of the field reported in Sect. 3 and Appendix A did not reveal any significant signal at the position of V838 Mon. These were however measurements mostly done with an integration time of 4 sec. Longer observations in a standard on-off mode, reported in Table 2 and displayed in Fig. 5, have however shown a clear emission. The line is very narrow and centered at a velocity very close to that of the SiO maser ( $V_{\text{LSR}} = 54.1 \text{ km s}^{-1}$ , Deguchi et al. 2005). In April 2005 we did not detect any emission in the (3→2) transition and an upper limit to  $T_{\text{mb}}$  of 0.25 K ( $3\sigma$ ) can be set up. More sensitive observations in December 2005 confirmed that the emission is also present in the (3→2) transition at the same velocity as the (2→1) component but about twice fainter.

Observations done in April 2006 revealed a significant emission not only at the position of V838 Mon but also at two offset positions, namely at (0, 1) and (0, -1). The obtained spectra are shown in Fig. 6, while the results of measurements can be found in Table 3. No significant emission has been

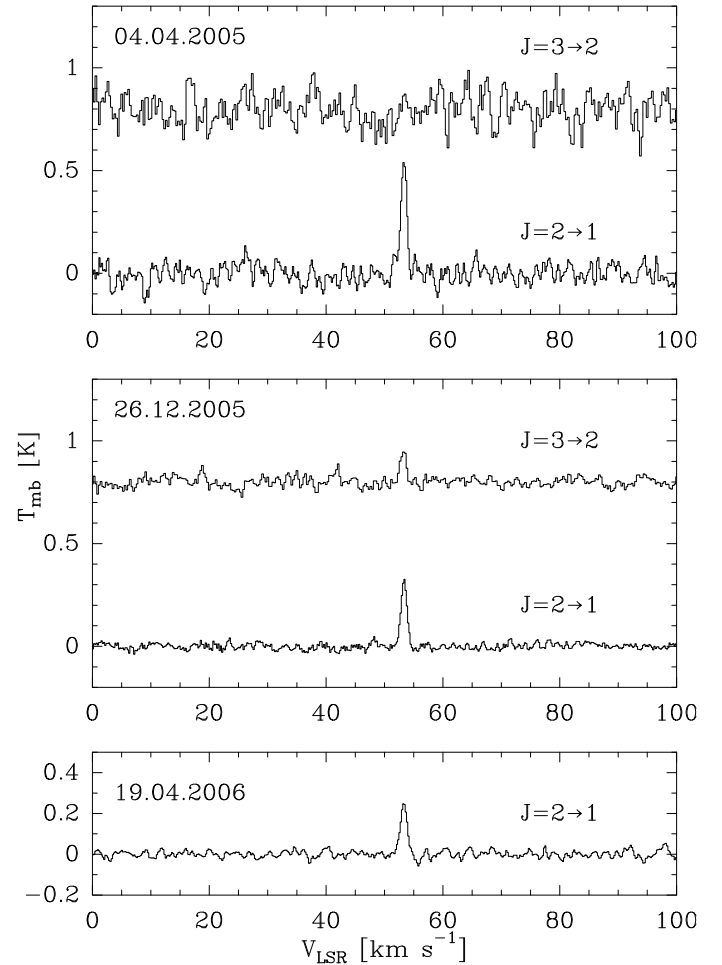


**Fig. 5.** Spectra in the CO (2→1) and (3→2) transitions obtained with the KOSMA telescope at the position of V838 Mon.

**Table 3.** Results of the CO (2→1) observations on 16-19 April 2006.

offset [arcmin]	$\sigma_{\text{rms}}$ [K]	$V_{\text{LSR}}$ [ $\text{km s}^{-1}$ ]	Peak $T_{\text{mb}}$ [K]	FWHM [ $\text{km s}^{-1}$ ]	$I_{\text{CO}}$ [ $\text{K km s}^{-1}$ ]
(0, 1)	0.052	53.3	0.251	0.82	0.220
(0, 0)	0.017	53.3	0.249	1.34	0.354
(0, -1)	0.027	53.0	0.139	2.00	0.297

detected in any of the other 4 offset positions and an upper limit to  $T_{\text{mb}}$  is 0.11 K ( $3\sigma$ ).

### 4.2. Results from the Delingha telescope

No emission has been detected at the V838 Mon position in the (1→0) transition and an upper limit to  $T_{\text{mb}}$  is 0.39 K ( $3\sigma$ ). Weak emission has been detected at three offsets and the results of measurements are in Table 4. The features are, however, at a level of  $\sim 2\sigma$ , so one can doubt if they are real. The feature at (0,1) is at the same velocity as the emissions seen in the (2→1) transition, which may argue that the feature is real. On the other hand the features in the two other offsets are at different velocities and wider than the lines observed in the (2→1) transition, which raises additional doubts about their reality.

**Table 2.** Results of the CO observations at the V838 Mon position with KOSMA.

date	line	HPBW [arcsec]	$T_{\text{sys}}$ [K]	$\Delta V_{\text{ch}}$ [km s <sup>-1</sup> ]	$\sigma_{\text{rms}}$ [K]	$V_{\text{LSR}}$ [km s <sup>-1</sup> ]	Peak $T_{\text{mb}}$ [K]	FWHM [km s <sup>-1</sup> ]	$I_{\text{CO}}^a$ [K km s <sup>-1</sup> ]
04.04.2005	2-1	130	168	0.21	0.043	53.3	0.553	1.17	0.691
	3-2	82	273	0.29	0.083	...	...	...	...
26.12.2005	2-1	130	310	0.21	0.014	53.3	0.323	1.18	0.406
	3-2	82	418	0.29	0.022	53.2	0.156	1.50	0.190
19.04.2006	2-1	130	397	0.21	0.017	53.3	0.249	1.34	0.354

<sup>a</sup> integrated intensity  $I_{\text{CO}} = \int T_{\text{mb}}(V) dV$

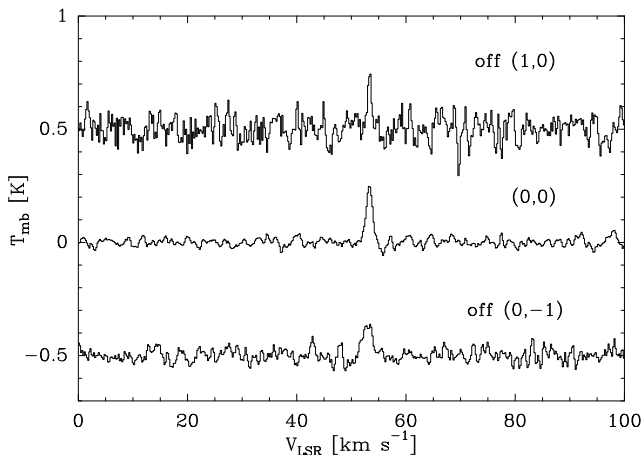


**Fig. 6.** Spectra in the CO (2→1) transition obtained on 16-19 April 2006 at the position of V838 Mon (middle) and at two offsets (in  $\alpha$  and  $\delta$  in arcmin).

**Table 4.** Results of the CO (1→0) observations obtained with the Delingha telescope on 28 Oct.–3 Nov. 2005.

offset [arcmin]	$\sigma_{\text{rms}}$ [K]	$V_{\text{LSR}}$ [km s <sup>-1</sup> ]	Peak $T_{\text{mb}}$ [K]	FWHM [km s <sup>-1</sup> ]	$I_{\text{CO}}$ [K km s <sup>-1</sup> ]
(0, 1)	0.39	53.5	0.83	2.79	2.46
(0, -1)	0.27	48.5	0.73	3.25	2.52
(1, -1)	0.35	48.2	0.53	7.49	4.20

## 5. Discussion and conclusions

Our on-the-fly maps in the CO rotational transitions, especially those done in the (2→1) line with the KOSMA telescope, have allowed us to identify 29 molecular clouds around the position of V838 Mon (see Appendix A). As far as we know, the region mapped with the KOSMA telescope has not been observed before with a sensitivity and a spatial resolution comparable to our survey. The data presented in Appendix A can be used in studies of molecular matter in the outer Galaxy.

We do not confirm the existence of a molecular bubble of a 1 degree dimension claimed in van Loon et al. (2004), which was probably an artefact resulted from merging two surveys of different resolution and sensitivity in the data used by van Loon et al.

Our maps did not reveal any molecular cloud in the near vicinity of V838 Mon. The nearest CO emission has been detected at ~40 arcmin from the position of the object (see Fig. 4). Thus the nearest dense molecular cloud is located at

least at a distance of ~80 pc from V838 Mon (assuming a 7 kpc distance to V838 Mon – see below). From the noise level in the (2→1) map (see Table 1) we can put an upper limit to  $I_{\text{CO}} = \int T_{\text{mb}} dV$  of 1.26 K km s<sup>-1</sup> ( $3\sigma_{\text{rms}}$ ) at the position of V838 Mon. Assuming the  $N(\text{H}_2)$  to  $I_{\text{CO}}$  conversion factor of  $X_{\text{CO}} = 5.1$  (in units  $10^{20}$  molecules cm<sup>-2</sup> K<sup>-1</sup> km<sup>-1</sup> s, typical value for the NC clouds discussed in Appendix A) we obtain an upper limit to the column density of  $N(\text{H}_2) = 6.4 \times 10^{20}$  cm<sup>-2</sup>. This upper limit is an order of magnitude lower than typical column densities observed for molecular clouds in the vicinity of the Sun (e.g. Blitz 1993). Thus we can conclude that V838 Mon is not located in a typical molecular cloud.

However, as presented in Sect. 4.1, long integrations in the on-off mode have allowed us to detect an emission in the CO (2→1) and (3→2) transitions at the position of V838 Mon. The question that arises is: what is the origin of this emission? Certainly it cannot come from the matter ejected in the 2002 outburst. That matter was expanding with large velocities, a few hundred km s<sup>-1</sup>, while our profiles have a FWHM of ~1 km s<sup>-1</sup>.

The  $V_{\text{LSR}}$  position and width of the CO lines similar to those of the SiO maser (Deguchi et al. 2005, Claussen et al. 2007) suggest that both emissions (CO and SiO) originate from the same place, e.g from the remnant of the 2002 outburst. However, in this case the KOSMA telescope would see a point source, which does not seem to be the case. The April 2006 observations show detectable emissions at the 1 arcmin offsets from the V838 Mon position (see Table 3). The HPBW of the KOSMA beam at 230 GHz is 130 arcsec. If the CO emission source were a point source at the (0,0) position, than the intensity measured at the (0,1) and (0, -1) offsets would be about twice fainter than that at the central position. Table 3 shows that this ratio is larger, i.e. 0.6 – 0.8. Unfortunately the accuracy of the measurements at the 1 arcmin offsets was not high, so we cannot say that the results in Table 3 are definitively inconsistent with a point source emission.

However, there are other arguments in favour of the idea that the CO emission is extended and/or situated outside the V838 Mon position. Our Delingha observations in the (1→0) transition (see Sect. 4.2) have not detected any emission at the V838 Mon position and the upper limit was 0.39 K. Assuming that the intensity in the (1→0) line is comparable to that in the (2→1) line (which is usually the case in molecular clouds) and that we observe a point source at the V838 Mon position than from the measured  $T_{\text{mb}}$  in the (2→1) transition in December 2005 (see Table 2), taking into account different beamsizes of the two telescopes (55 arcsec in Delingha versus 130 arcsec in KOSMA), the expected value of  $T_{\text{mb}}$  in the (1→0) Delingha observations would be ~1.8 K. This is 4.5 times higher than the observed upper limit. Thus either the (2→1)/(1→0) ratio is exceptionally large (> 4.5) or the CO source is situated

outside the Delingha beam but still inside the KOSMA beam. The later interpretation is supported by our possible detection of an emission with Delingha at three positions  $\sim 1$  arcmin from the object (see Table 4). It is also supported by a finding of Deguchi et al. (2007) who, using the Nobeyama telescope, tried to measure the CO (1 $\rightarrow$ 0) emission from a few points in a field around V838 Mon. A signal was detected from a position 30 arcsec north of V838 Mon at a velocity very close to that of the (2 $\rightarrow$ 1) line in our KOSMA observations. No emission was however recorded at the position of the object.

The above discussion allows us to conclude that the CO emission, clearly seen in our KOSMA observations, most probably originates not from V838 Mon itself but from a region (regions) situated, typically,  $\sim 1$  arcmin from the V838 Mon position. There are two possible ways of explaining the emission in this case. One is that the observed emission is a faint part of a larger CO structure belonging, for instance, to a molecular cloud. However, as discussed above, our CO maps have not revealed any dense CO cloud of similar  $V_{\text{LSR}}$  closer than  $\sim 40$  arcmin from the position of V838 Mon.

All the detected and possibly detected CO emission at and near the position of V838 Mon lie well within the optical light echo of V838 Mon. Hence the second possibility, namely that the CO emission comes from the same matter that gave rise to the light echo and that it was the light flash from the 2002 eruption which induced the emission. Then the observed narrowness of the line profile would be a strong argument that the matter is of interstellar origin rather than being ejected by V838 Mon in previous eruptions. The observed  $V_{\text{LSR}} = 53.3 \text{ km s}^{-1}$  of the CO emission would imply a kinematical distance of  $\sim 7.0$  kpc (using the Galactic rotational curve of Brandt & Blitz 1993). This can be compared to 6.1 – 6.2 kpc found by Bond et al. (2007) and  $\sim 8$  kpc advocated in Tylanda (2005).

Rushton et al. (2003) searched for CO emission from V838 Mon about a year after the 2002 eruption. No measurable signal was detected in the three lowest rotational transitions and the upper limit was  $T_A^* \lesssim 25 - 40 \text{ mK}$ . It is not straightforward to compare this result with our findings as the observations of Rushton et al. were done about 3 years before ours and the object probably evolved significantly during this time span. Nevertheless, given the beamwidth of the telescopes used by Rushton et al. (HPBW  $\leq 45''$ ), their negative result at the position of the object does not preclude a possibility that a significant emission was present in a near vicinity of the object, but outside the telescope beam.

More sensitive observations with a higher spatial resolution are required to distinguish between the above discussed possibilities and to further investigate the problem of the CO emission from V838 Mon.

*Acknowledgements.* We wish to thank all the staff at Delingha, the millimeter-wave radio telescope of Purple Mountain Observatory (China), for the observations in the CO (1 $\rightarrow$ 0) transition.

The KOSMA 3 m telescope is operated by the Kölner Observatorium für Submillimeter Astronomie of the I. Physikalisches Institut, Universität zu Köln in collaboration with the Radioastronomisches Institut, Universität Bonn.

The research reported in this paper was partly supported from a grant no. N203 004 32/0448 financed by the Polish Ministry of Science and Higher Education.

## References

Afsar, M. & Bond, H. E. 2007, *AJ*, 133, 387  
 Banerjee, D. P. K., Su, K. Y. L., Misselt, K. A., & Ashok, N. M. 2006, *ApJ*, 644, L57  
 Beuther, H., Kramer, C., Deiss, B., Stutzki, J. 2000, *A&A*, 362, 1109

Blitz, L. 1993, in *Protostars and Planets III*, eds. Levy, F. H. & Lunine, J. I., Univ. of Arizona Press, 125  
 Bond, H. E., Henden, A., Levay, Z. G., et al. 2003, *Nature*, 422, 405  
 Bond, H. E., Sparks, W. B., Cracraft, M. et al. 2006, *AAS Meeting Abstracts*, 209, #09.21  
 Bond, H. E. & Afsar, M. 2007, in *The Nature of V838 Mon and Its Light Echo*, eds. Corradi, R. L. M. & Munari, U., ASP Conference Series, 363, 241  
 Brandt, J. & Blitz, L. 1993, *A&A*, 275, 67  
 Brand, J., Wouterloot, J. G. A. 1995, *A&A*, 303, 851  
 Claussen, M., Bond, H. E., Starrfield, S., & Healy, K. 2007, in *The Nature of V838 Mon and Its Light Echo*, eds. Corradi, R. L. M. & Munari, U., ASP Conference Series, 363, 87  
 Crause, L. A., Lawson, W. A., Kilkenny, D., et al. 2003, *MNRAS*, 341, 785  
 Crause, L. A., Lawson, W. A., Menzies, J. W., & Marang, F. 2005, *MNRAS*, 358, 1352  
 Dame, T. M., Hartmann, D., & Thaddeus, P. 2001, *ApJ*, 547, 792  
 Deguchi, S., Matsunaga, N., & Fukushi, H. 2005, *PASJ*, 57, 933  
 Deguchi, S., Matsunaga, N., & Fukushi, H. 2007, in *The Nature of V838 Mon and Its Light Echo*, eds. Corradi, R. L. M. & Munari, U., ASP Conference Series, 363, 81  
 Digel, S. W., Bally, J., Thaddeus, P. 1990, *ApJ*, 357, 29  
 Graf, U. U., Honingh, C. E., Jacobs, K., Schieder, R., Stutzki, J. 1998, in *Astronomische Gesellschaft Meeting Abstracts*, 14, 120  
 Hasegawa, T. 1997, in *CO: Twenty-Five Years of Millimeter-Wave Spectroscopy*, eds. Latter, W. B., Radford, S. J. E., Jewell, P. R., Mangum, J. G. & Bally J., Kluwer, 39  
 Iben, I. Jr., & Tutukov, A. V. 1992, *ApJ*, 389, 369  
 Kamiński, T., Miller, M., Szczerba, R., & Tylanda, R. 2007, in *The Nature of V838 Mon and Its Light Echo*, eds. Corradi, R. L. M. & Munari, U., ASP Conference Series, 363, 103  
 Kimeswenger, S., Lederle, C., Schmeja, S., & Armsdorfer, B. 2002, *MNRAS*, 336, L43  
 Kramer, C., Beuther, H., Simon, R., Stutzki, J., & Winnewisser, G. 1999, in *Imaging at radio through submillimetre wavelength*, eds. Magnum, J. G. & Radford, S. J. E., Astronomical Society of Pacific, CF-217  
 Kramer, C., Degiacomi, Cuno G. et al. 1998, *SPIE*, 3357, 711K  
 Kutner, M. L., Ulich, B. L. 1981, *ApJ*, 250, 341  
 Lawlor, T. M. 2005, *MNRAS*, 361, 695  
 Maddalena, R. J., Morris, M., Moscovitz, J., Thaddeus, P. 1986, *ApJ*, 303, 375  
 MacLaren, I., Richardson, K. M., & Wolfendale, A. W. 1988, *ApJ*, 333, 821  
 Mead, K. N., Kutner M. L. 1988, *ApJ*, 330, 399  
 Munari, U., Henden, A., Kiyota, S., et al. 2002, *A&A*, 389, L51  
 Rohlfs, K. & Wilson, T. L. 2004, *Tools of Radio Astronomy*, forth edition, Springer  
 Rushton, M. T., Coulson, I. M., Evans, A. et al. 2003, *A&A*, 412, 767  
 Russeil, D. 2003, *A&A*, 397, 133  
 Schieder, R., Tolls, V., Winnewisser, G. 1989, *Exp. Astron.*, 1, 101  
 Sodroski, J. 1991, *ApJ*, 366, 95  
 Soker, N. & Tylanda, R. 2003, *ApJ*, 582, L105  
 Tylanda, R. 2004, *A&A*, 414, 223  
 Tylanda, R. 2005, *A&A*, 436, 1009  
 Tylanda, R., Soker, N., & Szczerba, R. 2005, *A&A*, 441, 1099  
 Tylanda, R. & Soker, N. 2006, *A&A*, 451, 223  
 Usuda, K. S., Hasegawa, T., Handa, T. et al. 1999, in *The Physics and Chemistry of the Interstellar Medium, Proceedings of the 3rd Cologne-Zermatt Symposium, held in Zermatt, September 22-25, 1998*, eds. Ossenkopf, V., Stutzki, J., & Winnewisser, G., GCA-Verlag Herdecke  
 van Loon, J. Th., Evans, A., Rushton, M. T., & Smalley, B. 2004, *A&A*, 427, 193

# Online Material

## Appendix A: Channel maps and the ISM cloud parameters

Figures A.1 – A.4 present channel maps integrated over narrow ranges in  $V_{\text{LSR}}$ . The data have been obtained with the KOSMA telescope. Details of the observations can be found in Sect. 2. The maps presented in Figs. A.1 and A.3 have been obtained in the  $^{12}\text{CO}$  ( $2 \rightarrow 1$ ) transition. The same but for the  $^{12}\text{CO}$  ( $3 \rightarrow 2$ ) transition is shown in Figs. A.2 and A.4.

As can be seen from Figs. A.1 – A.4 numerous more or less separate clouds of the CO emission can be distinguished. We have measured principal observational parameters of the clouds and the results are given in Table A.1. Column (1) gives the cloud number. The galactic ( $l$  and  $b$ ) and equatorial ( $\alpha_{2000}$  and  $\delta_{2000}$ ) coordinates of the geometric cloud centre are displayed in columns (2)–(5). The surface area of the cloud (in squared arcmin), determined from the  $J = 2 \rightarrow 1$  map, can be found in column (6). Columns (7), (8) and (9) give the total intensity integrated over the cloud surface (in  $\text{K km s}^{-1}$ ), the mean value of the cloud  $V_{\text{LSR}}$  and the FWHM of the velocity profile (both in  $\text{km s}^{-1}$ ), as measured in the  $J = 2 \rightarrow 1$  transition. The latter two values have been obtained from fitting a Gaussian profile to the  $V_{\text{LSR}}$  profile integrated over the cloud surface. The same three measurements, but obtained from the  $J = 3 \rightarrow 2$  map, are shown in columns (10), (11) and (12).

The upper part of Table A.1 lists clouds observed in the  $V_{\text{LSR}}$  range  $18 - 32 \text{ km s}^{-1}$ , called range P, later on. Those seen in the range  $44 - 57 \text{ km s}^{-1}$ , in the following called range NC, are given in the bottom part of the table. Note that in certain cases definition of an individual cloud is not obvious and can be subjective. Our goal was to delimit regions physically related. Therefore we have analysed not only the surface brightness distribution but also the surface distribution of  $V_{\text{LSR}}$  and attempted to single out structures concise in the space of both parameters. Small regions at the edge of our survey have not been included in Table A.1 as, probably, they are parts of larger structures lying outside the survey.

The data in Table A.1 allow us to estimate several important physical parameters of the CO clouds. The radial velocities can be used to estimate kinematic distances to the objects. For this purpose we have used the mean values of  $V_{\text{LSR}}$  derived from the  $J = 2 \rightarrow 1$  survey and listed in column (8). Note that the velocities derived from the  $J = 3 \rightarrow 2$  survey (column 11) do not significantly differ from the above ones. We have applied the Galactic rotational curve of Brandt & Blitz (1993) and the resultant heliocentric distances (in kpc) are given in column (13) in Table A.1. As can be seen from the results, the clouds in the  $V_{\text{LSR}}$  range P are typically at a distance of  $2.3 - 3.2 \text{ kpc}$  and form a different population from those in the range NC, which are at  $6.0 - 7.5 \text{ kpc}$ . These two populations can be easily identified with two outer Galactic arms, i.e. the Perseus arm and the Norma-Cygnus arm (Russeil 2003), respectively. (Hence our notation in the cloud numbers, P or NC, in Table A.1).

Assuming the virial theorem the mass of a molecular cloud can be estimated from (e.g. MacLaren et al. 1988)

$$M_{\text{vir}} = k_2 R \Delta V^2, \quad (\text{A.1})$$

where  $M_{\text{vir}}$  is the cloud mass in  $M_{\odot}$ ,  $R$  is the cloud radius in parsecs and  $\Delta V$  is the FWHM of the integrated line profile in  $\text{km s}^{-1}$ .  $k_2$  is a constant whose value depends on the density distribution in the cloud. Following a discussion of observational results for clouds in the outer Galaxy done in MacLaren et al. (1988) we assume an  $r^{-2}$  density distribution and  $k_2 = 126$ .

(Note that  $k_2$  rather weakly depends on the density distribution, e.g.  $k_2 = 190$  for  $\rho \sim r^{-1}$ .)

The cloud radius, as given in column (14) in Table A.1 (in pc), has been calculated from  $R = \sqrt{S/\pi}$ , where  $S$  is the cloud surface obtained from the measured angular surface given in column (6) and the distance in column (13) in Table A.1.

As can be seen from Table A.1, the velocity dispersion,  $\Delta V$ , in the  $J = 3 \rightarrow 2$  transition (column 12) is systematically lower than that in the  $J = 2 \rightarrow 1$  transition (column 9). Excluding the cloud NC3, for which the  $J = 3 \rightarrow 2$  profile is considerably affected by noise, the mean value and the standard deviation of  $\Delta V(3 - 2)/\Delta V(2 - 1)$  is  $0.86 \pm 0.12$ . Since the  $J = 3 \rightarrow 2$  transition is expected to be less optically thick than the  $J = 2 \rightarrow 1$  one, the above effect suggests that a certain line broadening due to optical thickness effects can be present. Therefore, following results of MacLaren et al. (1988), we have reduced the FWHM value from column (9) in Table A.1 by a factor of 0.7 when substituting to Eq. (A.1). The resultant cloud masses,  $M_{\text{vir}}$ , are given in column (12) in Table A.1 (in  $M_{\odot}$ ).

Another method of estimating the cloud mass is based on a conversion factor,  $X_{\text{CO}}$ , which allows one to derive the column density of  $\text{H}_2$  molecules along the line of sight from the observed CO velocity-integrated line intensity. The resultant mass,  $M_X$ , can then be obtained from

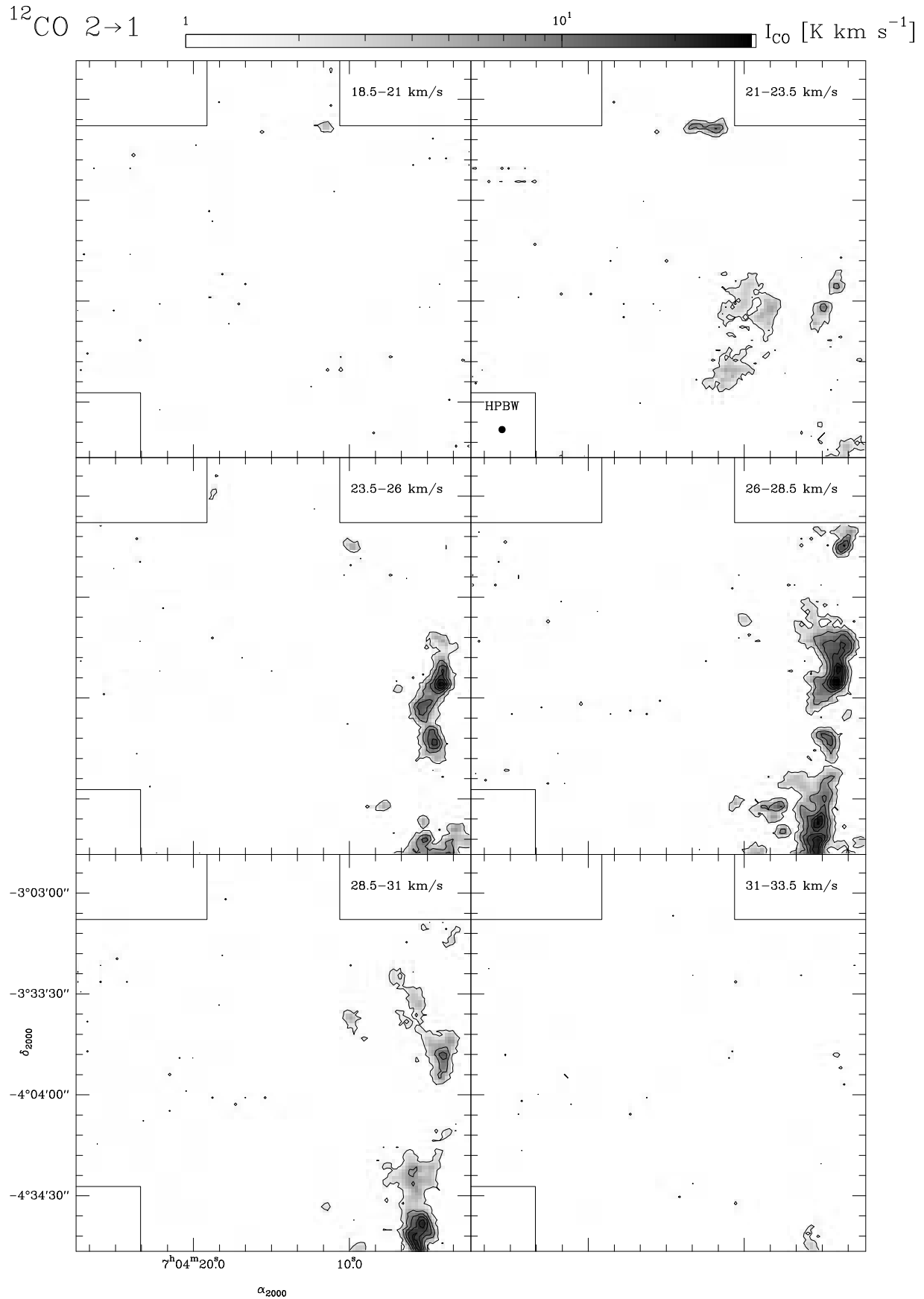
$$M_X = 1.4 m_{\text{H}_2} X_{\text{CO}} W_{\text{CO}} d^2, \quad (\text{A.2})$$

where  $W_{\text{CO}}$  is the line intensity integrated over the velocity and the cloud surface, while  $d$  is the distance.  $m_{\text{H}_2}$  is the mass of an  $\text{H}_2$  molecule and the factor of 1.4 corrects for helium. Note that  $X_{\text{CO}}$  is usually meant to convert intensities in the CO  $J = 1 \rightarrow 0$  line, whereas our measurements were done in the  $J = 2 \rightarrow 1$  line. However, as observations of molecular clouds show, the ratio of the two lines is usually close to 1.0 (e.g. Brand & Wouterloot 1995, Hasegawa 1997). Therefore we can directly use our measurements of  $W_{\text{CO}}$  given in column (7) in Table A.1 when calculating the cloud masses from Eq. (A.2).

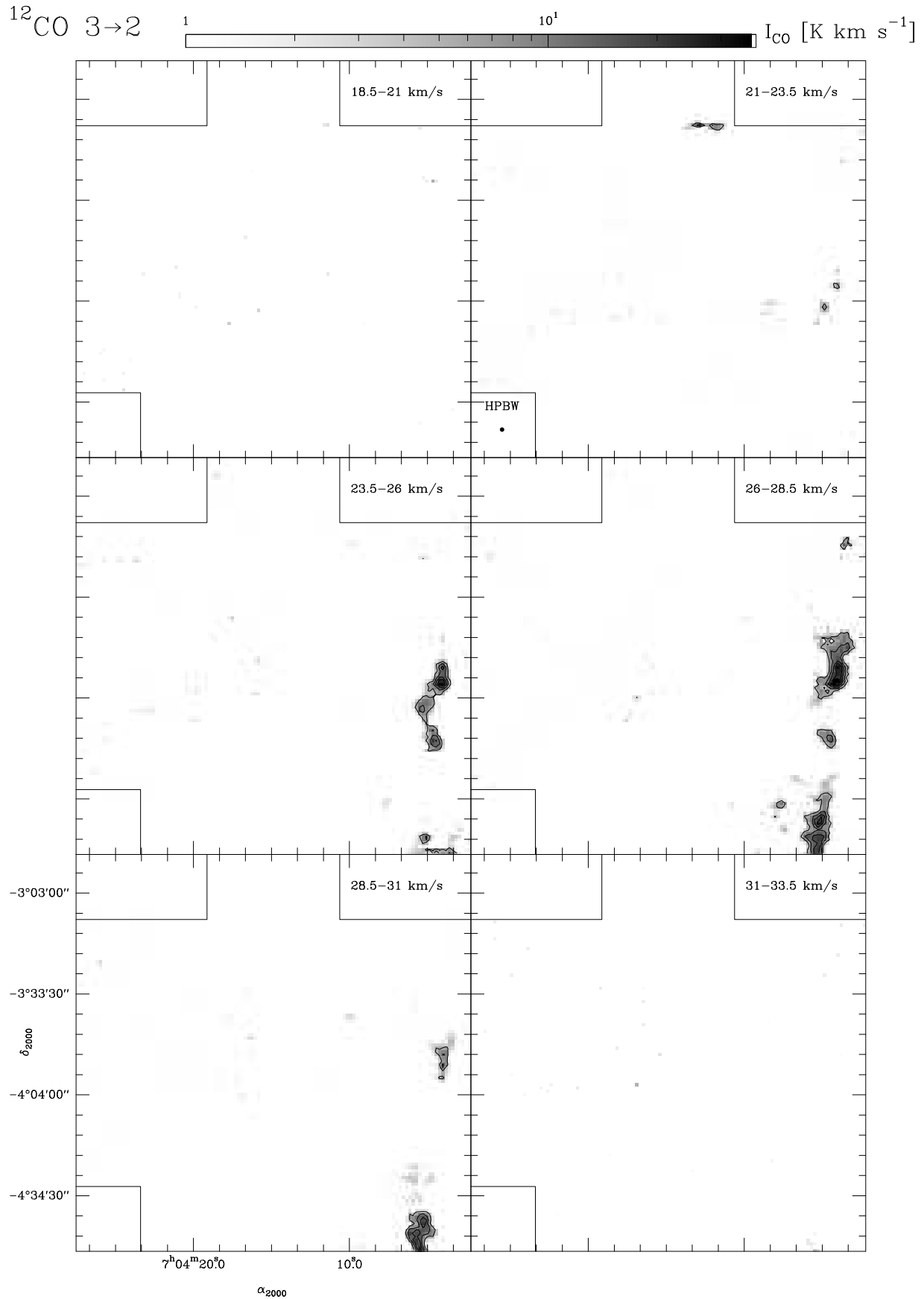
There are numerous estimates of the value of  $X_{\text{CO}}$  in the literature. For the inner Galaxy they are close to 1.0 (in units  $10^{20} \text{ molecules cm}^{-2} \text{ K}^{-1} \text{ km}^{-1} \text{ s}$ ) (e.g. MacLaren et al. 1988, Maddalena et al. 1986). In the outer Galaxy  $X_{\text{CO}}$  is usually larger (Mead & Kutner 1988, Digel et al. 1990, Sodrski 1991, Usuda et al. 1999). We assume, as a working value,  $X_{\text{CO}} = 1.0$ . The resultant cloud masses (in  $M_{\odot}$ ) obtained from Eq. (A.2) and using the values from columns (7) and (13) in Table A.1 can be found in the last column of the table.

Fig. A.5 compares the resultant clouds masses determined from the above two methods. As can be seen, for all the clouds  $M_{\text{vir}}$  is greater than  $M_X$ . This is in accord with the above note that in the outer Galaxy  $X_{\text{CO}}$  is expected to be greater than 1. The clouds from the Perseus arm, however, suggest a linear relation in Fig. A.5 (see asterisks) with a slope greater than 1. The observed position in the figure can be fitted by  $\log M_X = -1.67 + 1.40 \log M_{\text{vir}}$ , which can be transformed to  $X_{\text{CO}} = M_{\text{vir}}/M_X = 2.2(M_X/10^3 M_{\odot})^{-0.29}$ . Note, however, that the statistics is poor and the above relation relies on a few extreme points in Fig. A.5. No similar relation is seen for the Norma-Cygnus arm clouds (open points in Fig. A.5). A mean value of the shift of the open points from the full line in Fig. A.5 corresponds to  $X_{\text{CO}} = 5.1$ . This result is close to the value found for the outer Galaxy by Usuda et al. 1999, i.e.  $X_{\text{CO}} = 5.4 \pm 0.5$ . In the NC population we do not see clouds of a mass as low as some of the P clouds. If a similar mass range is considered in both populations, i.e. when the 5 least massive P clouds are not

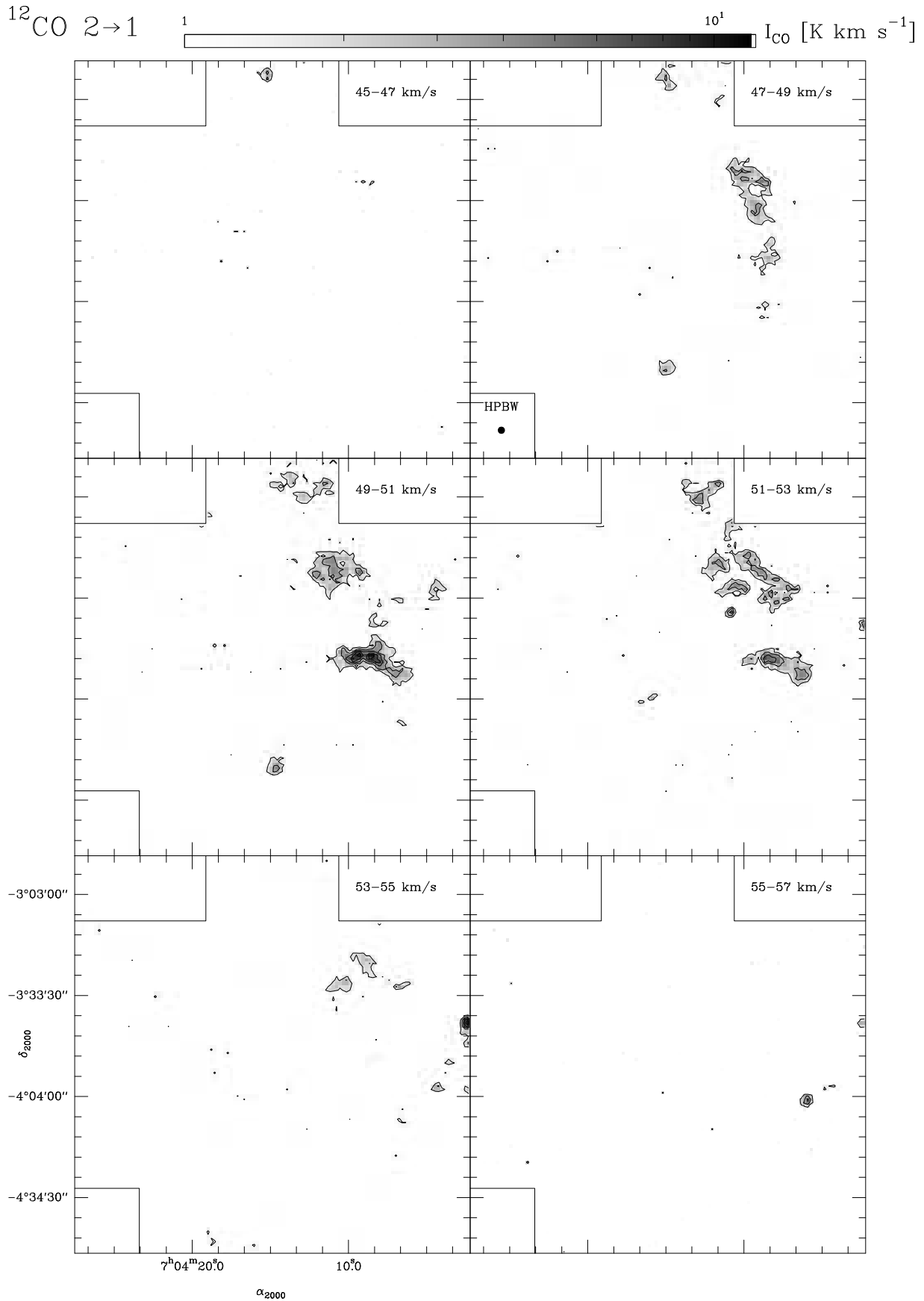




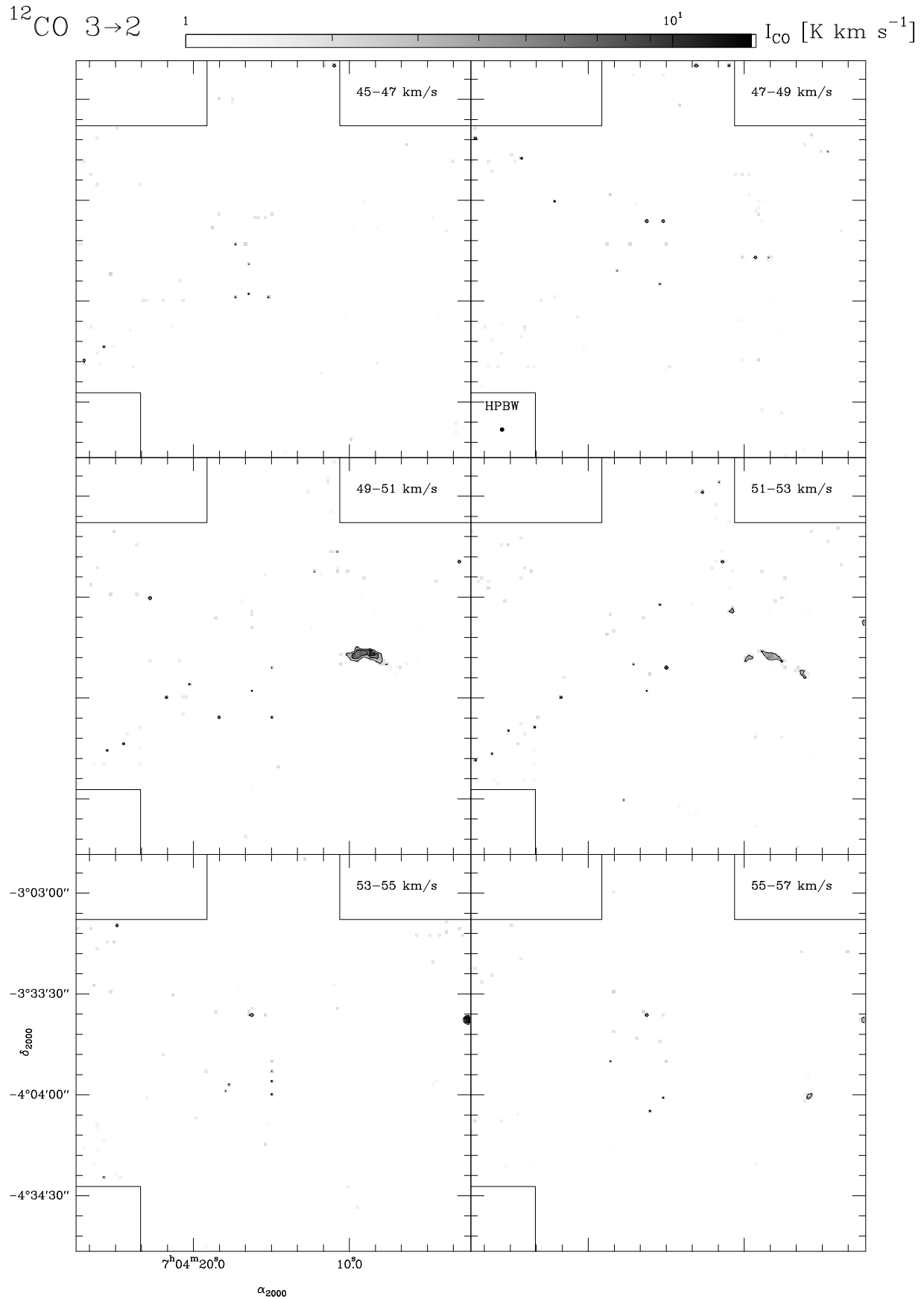
**Fig. A.1.** Channel maps of  $^{12}\text{CO } (2 \rightarrow 1)$  integrated intensity for the velocity range P (18–33.5 km s $^{-1}$ ) in a step of 2.5 km s $^{-1}$ . The integration range is given at the upper right corner of each map. Countours are plotted from 1.6 to 31.1 K km s $^{-1}$  by 4.9 K km s $^{-1}$  (5 to 95% by 15% of the maximum for all the six maps.)



**Fig. A.2.** Channel maps of  $^{12}\text{CO } (3\rightarrow 2)$  integrated intensity for the velocity range P (18–33.5 km s $^{-1}$ ) in a step of 2.5 km s $^{-1}$ . The integration range is given at the upper right corner of each map. Countours are plotted from 5.6 to 33.7 K km s $^{-1}$  by 5.6 K km s $^{-1}$  (15 to 95% by 15% of the maximum value for all the six maps.)



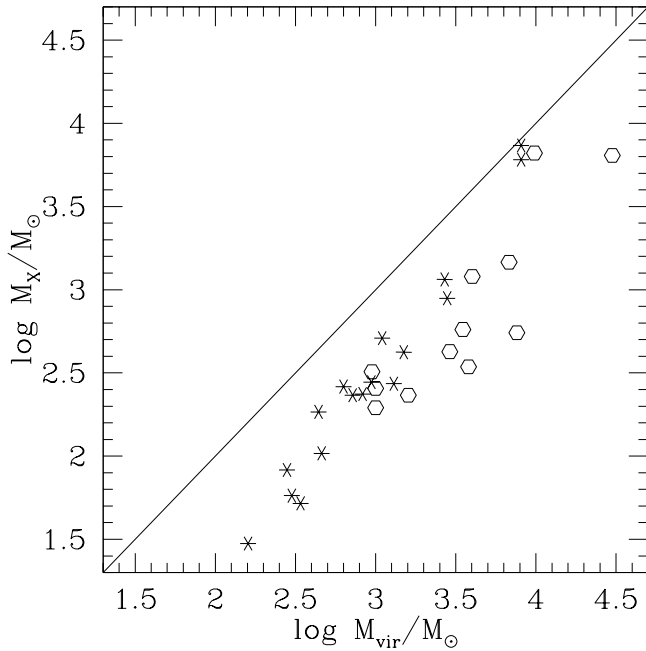
**Fig. A.3.** Channel maps of  $^{12}\text{CO}$  ( $2 \rightarrow 1$ ) integrated intensity for the velocity range NC ( $45\text{--}57 \text{ km s}^{-1}$ ) in a step of  $2 \text{ km s}^{-1}$ . The integration range is given at the upper right corner of each map. Countours are plotted from  $1.6$  to  $10.6 \text{ K km s}^{-1}$  by  $1.8 \text{ K km s}^{-1}$  (13 to 88% by 15% of the maximum for all the six maps.)



**Fig. A.4.** Channel maps of  $^{12}\text{CO } (3 \rightarrow 2)$  integrated intensity for the velocity range NC (45–57 km s $^{-1}$ ) in a step of 2 km s $^{-1}$ . The integration range is given at the upper right corner of each map. Countours are plotted from 2.2 to 14.2 K km s $^{-1}$  by 3 K km s $^{-1}$  (15 to 95% by 20% of the maximum for all the six maps.)

**Table A.1.** Measured and calculated parameters for individual clouds in the V838 Mon field. See text for the explanations of the columns.

nr (1)	$l$ (2)	$b$ (3)	$\alpha_{2000}$ (4)	$\delta_{2000}$ (5)	$A$ (6)	$W_{2-1}$ (7)	$V_{2-1}$ (8)	$\Delta V_{2-1}$ (9)	$W_{3-2}$ (10)	$V_{3-2}$ (11)	$\Delta V_{3-2}$ (12)	$d$ (13)	$R$ (14)	$M_{\text{vir}}$ (15)	$M_X$ (16)
P1	217.07	0.74	06:59:08.5	-03:16:06.2	61	328.3	27.7	2.16	77.3	28.0	1.88	3.0	3.8	1100	510
P2	217.33	1.39	07:01:55.5	-03:11:47.6	67	282.2	21.9	1.83	159.3	22.0	1.71	2.3	3.1	630	260
P3	217.33	1.17	07:01:08.7	-03:18:04.8	22	50.3	24.2	1.56				2.6	2.0	300	58
P4	217.37	0.89	07:00:12.5	-03:28:19.1	33	46.8	29.2	1.24				3.2	3.0	280	83
P5	217.44	0.74	06:59:48.0	-03:35:51.8	61	162.6	28.8	1.95	24.9	28.9	1.28	3.1	4.0	940	280
P6	217.61	0.52	06:59:21.3	-03:50:46.3	347	4093.0	27.0	3.84	2568.1	27.0	3.46	2.9	8.8	8100	6000
P7	217.68	0.97	07:01:05.7	-03:42:30.5	44	108.5	28.7	1.46	27.6	28.7	1.03	3.1	3.4	440	180
P8	217.90	0.45	06:59:38.5	-04:08:11.7	82	732.0	24.8	3.42	423.5	24.7	3.36	2.6	3.9	2800	890
P9	218.01	0.84	07:01:14.3	-04:03:20.7	133	234.0	22.7	1.61	19.9	22.8	1.45	2.4	4.5	720	230
P10	218.01	0.70	07:00:43.3	-04:07:39.4	115	250.2	22.1	1.82	55.5	22.2	1.61	2.3	4.1	830	240
P11	218.02	0.35	06:59:29.1	-04:17:32.1	100	887.4	25.5	3.14	533.7	25.5	2.85	2.7	4.4	2700	1200
P12	218.32	0.25	06:59:43.3	-04:36:34.6	421	4472.5	28.2	3.59	2463.9	28.3	3.36	3.1	10.3	8100	7400
P13	218.34	0.74	07:01:27.9	-04:23:49.4	151	291.2	22.0	2.10	16.7	22.0	1.70	2.3	4.6	1300	270
P14	218.45	0.45	07:00:38.8	-04:37:50.0	70	285.2	27.0	2.48	106.5	27.0	2.20	2.9	4.0	1500	420
P15	218.49	0.61	07:01:19.3	-04:35:31.4	17	35.2	27.0	1.69				2.9	2.0	340	52
P16	218.51	0.34	07:00:23.7	-04:44:07.2	19	67.9	27.5	1.88	19.6	27.3	1.79	2.9	2.1	460	100
P17	218.56	0.67	07:01:39.6	-04:37:20.1	12	17.1	29.0	1.19				3.1	1.8	160	30
NC1	217.17	1.62	07:02:25.8	-02:57:20.3	52	80.1	49.2	4.09				6.2	7.4	7600	550
NC2	217.18	1.73	07:02:51.7	-02:54:43.2	31	56.9	47.1	3.40				5.9	5.3	3800	340
NC3	217.19	1.47	07:01:56.4	-03:02:34.5	100	191.4	50.9	3.19	23.0	50.6	5.43	6.6	10.8	6800	1500
NC4	217.32	0.68	06:59:23.2	-03:31:12.2	25	27.1	49.9	1.77				6.4	5.2	1000	200
NC5	217.45	0.90	07:00:24.0	-03:32:25.6	69	147.8	52.0	2.66	14.2	51.2	2.97	6.8	9.2	4000	1200
NC6	217.46	1.15	07:01:18.6	-03:25:47.6	258	850.4	50.7	5.33	69.3	50.1	4.01	6.5	17.2	30000	6400
NC7	217.57	0.96	07:00:51.3	-03:36:47.4	78	36.0	48.1	1.72	27.2	47.9	1.38	6.0	8.8	1600	230
NC8	217.65	1.10	07:01:29.1	-03:37:29.3	15	30.7	52.4	1.95				6.9	4.4	1000	260
NC9	217.76	0.45	06:59:21.6	-04:01:03.3	24	33.6	54.7	1.61				7.4	5.9	950	320
NC10	217.77	0.80	07:00:38.6	-03:51:37.7	250	900.9	50.3	3.08	285.0	50.3	2.63	6.5	16.7	9800	6600
NC11	217.90	0.54	06:59:57.3	-04:06:07.0	20	42.4	55.5	2.92	13.6	56.1	1.57	7.5	5.5	2900	420
NC12	218.48	1.01	07:02:43.1	-04:23:55.3	47	83.5	49.2	2.85	9.6	49.3	2.49	6.3	7.0	3500	580

**Fig. A.5.**  $M_X$  (derived from Eq. A.2, see column 16 in Table A.1), plotted versus  $M_{\text{vir}}$  (derived from Eq. A.1, see column 15 in Table A.1). Asterisks: P clouds, open symbols: NC clouds. The full line shows a 1:1 relation.

taken into account, then a mean value of  $X_{\text{CO}} = 2.6$  is obtained for the Perseus arm clouds.